Inorganic Chemistry

Article

pubs.acs.org/IC

Multinuclear Copper(I) and Silver(I) Amidinate Complexes: Synthesis, Luminescence, and CS_2 Insertion Reactivity

Andrew C. Lane,[†] Matthew V. Vollmer,[†] Charles H. Laber,[†] Doris Y. Melgarejo,[‡] Gina M. Chiarella,[‡] John P. Fackler, Jr.,[‡] Xinzheng Yang,[§] Gary A. Baker,[†] and Justin R. Walensky*[,†]

[†]Department of Chemistry, University of Missouri, 601 S. College Avenue, Columbia, Missouri 65211, United States

[‡]Department of Chemistry, Texas A&M University, P.O. Box 3255, College Station, Texas 77843, United States

[§]Beijing National Laboratory for Molecular Sciences, State Key Laboratory for Structural Chemistry of Unstable and Stable Species, Institute of Chemistry, Chinese Academy of Sciences, Beijing 100190, China

Supporting Information

ABSTRACT: Dinuclear Cu(I) and Ag(I) complexes, $Cu_2[(2,6\text{-}Me_2C_6H_3N)_2C(H)]_2$, **1**, $Ag_2[(2,6\text{-}Me_2C_6H_3N)_2C(H)]_2$, **2**, $Cu_2[2,6\text{-}^iPr_2C_6H_3N)_2C(H)]_2$, **3**, and $Ag_2[(2,6\text{-}^iPr_2C_6H_3N)_2C(H)]_2$, **4**, were synthesized from reactions of $[Cu(NCCH_3)_4][PF_6]$ with $Na[(2,6\text{-}R_2C_6H_3N)_2C(H)]$ and AgO_2CCH_3 with $[Et_3NH][(2,6\text{-}R_2C_6H_3N_2C(H)]$, R = Me, ^{i}Pr. Carbon disulfide was observed to insert into the metal−nitrogen bonds of **1** to produce $Cu_4[CS_2(2,6\text{-}Me_2C_6H_3NC(H)=NC_6H_3Me_2)]_4$, **5**, with a Cu_4S_8 core, which represents a rare transformation of dinuclear to tetranuclear species. Insertion is also observed with **2** and CS_2, with the product likely being polymeric, **6**. With the ^{i}Pr-derivatives, CS_2 insertion was also observed, albeit at much slower rate, with **3** and **4** producing hexanuclear clusters, $M_6[CS_2(2,6\text{-}Me_2C_6H_3NC(H)=NC_6H_3Me_2)]_6$, M = Cu, **7**; Ag, **8**. Complexes **1** and **5** display green luminescence, a feature not shared by their Ag(I) analogs nor with **3**. Notably, oxygen acts as a collisional quencher of the luminescence from **1** and **5** at a rate faster than most metal-based quenchometric O_2 sensors. For example, we find that complex **1** can be rapidly and reversibly quenched by oxygen, presenting a nearly 6-fold drop in intensity upon switching from nitrogen to an aerated atmosphere. The results here provide a platform from which further group 11 amidinate reactivity can be explored.

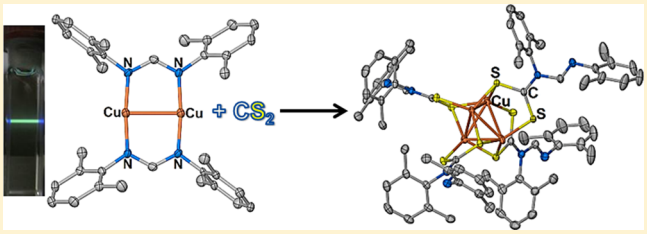

INTRODUCTION

The properties of the coinage metals are unique compared to the rest of the periodic table. For example, group 11 metals show metallophilic interactions[1,2] in which metal−metal interactions are atypically shorter than the sum of their van der Waals radii. This can lead to enhanced photophysical properties[3−5] as well as stabilization of metal complexes. In particular, gold−gold interactions, or aurophilicity,[6] have been approximated to have the strength of hydrogen bonding. Most intriguing is that the origin of this interaction remains unresolved and is an area being actively investigated today.[7,8] Dinuclear group 11 complexes in particular offer the opportunity to study the reactivity of two metal centers in close proximity to each other. One application for this is in cytochrome *c* oxidase in which the Cu_A site contains a Cu(I,I) dinuclear core with a short Cu−Cu bond distance, and with Cu−N bonds from histidine as well as Cu−S bonds from cysteine residues.[9]

Group 11 amidinate complexes were identified many years ago.[10−21] The alkyl derivatives have been shown as promising precursors for atomic layer deposition (ALD) due to their low melting point, low deposition temperature, and their ability to afford pure films. Similar amidinate ligands to the ones used in this study have yielded di- and tetranuclear copper(I) clusters.[22,23] Silver amidinate complexes have also been made, but are less common.[24−28] In 2005, the synthesis of the Au(I) formamidinate, $Au_2[(2,6\text{-}Me_2C_6H_3N)_2C(H)]_2$, was reported,[15] and its oxidative chemistry was shown to be reminiscent of previously reported work by Schmidbaur with gold ylide complexes.[29] On the other hand, the reaction chemistry of copper and silver amidinate complexes remains virtually unexplored.

With this in mind, our primary objective in the current work is to synthesize new copper(I) and silver(I) amidinate complexes with emphasis on exploring their reactivity when two metal centers lie in close proximity. It is noteworthy that no reaction chemistry with dinuclear group 11 amidinate complexes has been reported besides oxidative chemistry with $Au_2[(2,6\text{-}Me_2C_6H_3N)_2C(H)]_2$. Here, we report the synthesis and X-ray structures of four new Cu(I) and Ag(I) amidinate complexes, their luminescence, and reactivity with carbon disulfide.

Received: January 28, 2014
Published: October 15, 2014

   dx.doi.org/10.1021/ic501694d | *Inorg. Chem.* 2014, 53, 11357−11366

EXPERIMENTAL SECTION

General Considerations. The syntheses described here with Ag(I) were carried out on the benchtop while all Cu(I) reactivity was done under inert atmosphere (N_2) using glovebox (Vacuum Atmospheres OMNI) or standard Schlenk techniques. Solvents were distilled under nitrogen and stored over drying sieves. $NaN(SiMe_3)_2$, $KN(SiMe_3)_2$, anhydrous CS_2, AgO_2CCH_3 (Aldrich), and $[Cu(NCMe)_4][PF_6]$ (Strem) were used as received. The formamidine ligands were prepared as previously described.[30] NMR spectroscopy experiments were conducted with a Bruker 300 or 500 MHz spectrometer. ^1H and ^{13}C NMR chemical shifts were verified using hetero-multinuclear quantum correlation (HMQC) spectroscopy. Elemental analysis was performed by Atlantic Microlab (Norcross, GA). Absorbance spectra were obtained using a Varian Cary 50 Bio UV−vis spectrophotometer, and luminescence spectra were acquired on a Varian Cary Eclipse fluorimeter.

Synthesis of $Cu_2[(2,6\text{-}Me_2C_6H_3N)_2C(H)]_2$, 1. $NaN(SiMe_3)_2$ (79 mg, 0.43 mmol) was added to a stirred solution of 2,6-dimethylphenylformamidine (100 mg, 0.396 mmol) in THF (15 mL). After 1 h, $[Cu(NCMe)_4][PF_6]$ (147 mg, 0.396 mmol) was added and allowed to stir for 12 h. Insoluble material was removed by centrifugation, and the solvent was removed under vacuum to yield **1** as a white powder (181 mg, 74%). X-ray quality crystals were grown overnight from a saturated toluene solution at −25 °C. ^1H NMR ($CDCl_3$, 300 MHz): δ 7.13 (d, $^3J_{H-H}$ = 7.5 Hz, 8H, Ph), 7.10 (t, $^3J_{H-H}$ = 7.5 Hz, 4H, Ph), 6.86 (s, 2H, CH), 2.57 (s, 24H, Me) ppm. ^{13}C NMR ($CDCl_3$, 125 MHz): δ 170.4 (CH), 148.8 (quat C, Ph), 132.9 (Ph), 128.6 (Ph), 124.6 (Ph), 19.5 (CH_3) ppm. IR (KBr): 2975 (m), 2949 (m), 2919 (m), 1635 (m), 1599 (s), 1464 (s), 1336 (s), 836 (s), 766 (s) cm^{-1}. Elemental Anal. Calcd for $C_{34}H_{38}N_4Cu_2$: C, 64.84%; H, 6.08%; N, 8.90%. Found: C, 65.01%; H, 5.89%; N, 9.04%.

Synthesis of $Ag_2[(2,6\text{-}Me_2C_6H_3N)_2C(H)]_2$, 2. To a stirred solution of 2,6-dimethylphenylformamidine (151 mg, 0.60 mmol) was added triethylamine (101 mg, 1.80 mmol) in methanol (10 mL). After 10 min, a solution of silver acetate (100 mg, 0.60 mmol) in 10 mL of dichloromethane was added. The reaction mixture was heated at 40 °C for 10 min, and then filtered through Celite and allowed to stand undisturbed at −25 °C overnight. Product **2** was gathered as colorless crystals (159 mg, 74%). X-ray quality crystals were grown overnight from a saturated CH_2Cl_2/MeOH solution at −25 °C. ^1H NMR ($CDCl_3$, 500 MHz): δ 7.28 (t, 2H, $^3J_{H-Ag}$ = 16.2 Hz, CH), 7.01 (d, 8H, $^3J_{H-H}$ = 7.5 Hz, Ph), 6.90 (t, $^3J_{H-H}$ = 7.0 Hz, Ph), 2.34 (s, 24H, Me) ppm. ^{13}C NMR ($CDCl_3$, 125 MHz): δ 166.3 (CH), 148.8 (Ph), 132.90 (Ph), 128.3 (Ph), 124.0 (Ph), 19.65 (CH_3) ppm. IR (KBr): 3011 (m), 2974 (m), 2943 (m), 1597 (s), 1560 (vs), 1467 (m), 1382 (m), 1339 (m), 1197 (m), 762 (m) cm^{-1}. Elemental Anal. Calcd for $C_{34}H_{38}N_4Ag_2$: C, 56.84%; H, 5.33%; N, 7.80%. Found: C, 56.56%; H, 5.63%; N, 7.71%.

Synthesis of $Cu_2[(2,6\text{-}^iPr_2C_6H_3N)_2C(H)]_2$, 3. To a stirred solution of 2,6-diisopropylphenylformamidine (100 mg, 0.278 mmol) was added $KN(SiMe_3)_2$ (57 mg, 0.29 mmol) in THF (15 mL). After 1 h, $[Cu(NCMe)_4][PF_6]$ (107 mg, 0.287 mmol) was added and allowed to stir for 12 h. Insoluble material was removed by centrifugation and the solvent removed under vacuum to yield **1** as a white powder (140 mg, 57%). X-ray quality crystals were grown overnight from a saturated toluene solution at −25 °C. ^1H NMR (C_6D_6, 300 MHz): δ 7.06 (t, 8H, $^3J_{H-H}$ = 5.4 Hz, Ph), 7.03 (d, 4H, $^3J_{H-H}$ = 5.4 Hz, Ph), 6.97 (s, 2H, CH), 3.78 (sept, 8H, $^3J_{H-H}$ = 6.9 Hz, CH), 1.26 (d, 12H, $^3J_{H-H}$ = 6.9 Hz, Me), 1.22 (d, 12H, $^3J_{H-H}$ = 6.9 Hz, Me) ppm. ^{13}C NMR (C_6D_6, 125 MHz): δ 169.6 (CH), 125.4 (Ph), 123.3 (Ph), 30.2 (Me), 23.7 (Me) ppm. IR (KBr): 3070 (w), 3040 (w), 2958 (s), 2867 (m), 1631 (m), 1595 (s), 1463 (m), 1436 (m), 1383 (s), 1320 (m), 801 (m), 756 (m), 562 (s) cm^{-1}. Elemental Anal. Calcd for $C_{50}H_{70}N_4Cu_2$: C, 70.30%; H, 8.26%; N, 6.56%. Found: C, 70.51%; H, 8.41%; N, 6.87%.

Synthesis of $Ag_2[(2,6\text{-}^iPr_2C_6H_3N)_2C(H)]_2$, 4. To a stirred solution of 2,6-diisopropylphenylformamidine (0.940 g, 2.6 mmol) in 50 mL of dichloromethane was added triethylamine (0.783 g, 7.70 mmol). The reaction mixture was brought to a boil on a stir plate, and silver acetate (0.430 g, 2.6 mmol) was added and allowed to stir until all the silver acetate had been consumed (5−10 min). The reaction was then filtered hot over a coarse porosity fritted filter packed with 1 in. of Celite. The mixture was allowed to reach room temperature, then carefully layered with 100 mL of methanol, and the mixture stored at −20 °C after agitation. Over the course of 1 h the product precipitated as an analytically pure colorless semicrystalline powder (700 mg, 60%). Another fraction could be obtained by placing the material again at −20 °C for 2 days. X-ray quality crystals were grown from a saturated dichoromethane/methanol solution. ^1H NMR (C_7D_8, 300 MHz): δ 7.22 (dt-dd, 2H, $^3J_{Ag109-H}$ = 18.0 Hz, $^3J_{Ag107-H}$ = 15.9 Hz, $^3J_{Ag109/107-H}$ = 17.1 Hz, 18.0 Hz, CH), 7.1−7.0 (m, 12H, Ph), 3.72 (sept, 4H, $^3J_{H-H}$ = 6.9 Hz, CH), 1.19 (d, 12H, $^3J_{H-H}$ = 6.9 Hz, Me), 1.17 (d, 12H, $^3J_{H-H}$ = 6.9 Hz, Me) ppm. ^{13}C NMR (CD_2Cl_2, 125 MHz): δ 166.4 (C=N), 146.4 (Ph), 144.0 (Ph), 125.1 (Ph), 123.4 (Ph), 28.01 ($(CH(CH_3)_2)$), 24.31 ($CH(CH_3)_2$), 23.67 ($CH(CH_3)_2$) ppm. IR (KBr): 3060 (w), 3025 (w), 2960 (vs), 2866 (vs), 1664 (m), 1595 (s), 1554 (vs), 1462 (s), 1439 (s), 1382 (s), 1337 (s), 933 (m), 802 (m), 755(s), 725 (w), 415 (w) cm^{-1}. Anal. Calcd for $C_{50}H_{70}Ag_2N_4{\cdot}2CH_3OH{\cdot}0.5CH_2Cl_2$: C, 60.46%; H, 7.63%; N, 5.38%. Found: C, 60.75%; H, 7.23%; N, 5.58%.

Synthesis of $Cu_4[CS_2(2,6\text{-}Me_2C_6H_3NC(H)=NC_6H_3Me_2)]_4$, 5. To a stirred solution of **1** (200 mg, 0.223 mmol) in 8 mL of THF was added an excess amount of CS_2 (~0.1 mL). The color of the solution immediately changed from colorless to orange. After 30 min, the solvent was removed under vacuum to yield a yellow powder (164 mg, 44%). X-ray quality crystals of **5** were obtained from a saturated THF solution at −25 °C. ^1H NMR (C_6D_6, 300 MHz): δ 9.42 (s, 2H, CH), 7.25 (m, 6H, Ph), 7.16 (d, 4H, $^3J_{H-H}$ = 7.5 Hz, Ph), 6.97 (d, 4H, $^3J_{H-H}$ = 7.5 Hz, Ph), 6.87 (t, 2H, $^3J_{H-H}$ = 7.5 Hz, Ph), 2.20 (s, 12H, CH_3), 2.06 (s, 12H, CH_3) ppm. ^{13}C NMR (C_6D_6, 125 MHz): δ 150.1 (methine), 147.1 (quat), 140.0 (quat), 135.1 (quat), 129.0 (Ph), 128.5 (Ph), 128.1 (Ph), 127.6 (Ph), 124.0 (quat), 18.7 (CH_3), 18.1 (CH_3) ppm. IR (KBr): 3121 (s), 2948 (s), 2843 (s), 1643 (m), 1384 (s), 838 (s), 766 (m) 563 (m) cm^{-1}. Elemental Anal. Calcd for $C_{72}H_{80}N_8S_8Cu_4$: C, 55.15%; H, 5.14%; N, 7.15%. Found: C, 54.82%; H, 4.99%; N, 7.03%.

Reaction of 2 with CS_2, 6. To a stirred solution of **2** (100 mg, 0.140 mmol) in 10 mL of $CHCl_3$ was added an excess amount of CS_2 (~0.1 mL). The solution was allowed to stir at room temperature overnight and the color progressed from colorless to bright yellow. After this time, 15 mL of diethyl ether was added, and a yellow powder precipitated from the solution. The precipitate was gathered by vacuum filtration (20 mg). ^1H NMR ($CDCl_3$, 500 MHz): δ 9.46 (s, 2H), 7.25 (t, 2H, $^3J_{H-H}$ = 7.5 Hz), 7.17 (d, 4H, $^3J_{H-H}$ = 7.5 Hz), 6.96 (d, 4H, $^3J_{H-H}$ = 7.5 Hz), 6.87 (t, 2H, $^3J_{H-H}$ = 7.5 Hz), 2.17 (s, 12H), 2.04 (s, 12H) ppm. ^{13}C NMR ($CDCl_3$, 125 MHz): δ 151.0 (quat), 147.1 (methine), 140.8 (quat), 135.06 (methine), 129.0 (quat), 128.7 (Ph), 128.3 (Ph), 127.8 (Ph), 124.12 (quat), 18.9 (CH_3), 18.3 (CH_3) ppm. IR (KBr): 3063 (m), 3012 (m), 2992 (m), 2853 (m), 1644 (s), 1596 (s), 1559 (vs), 1467 (vs), 1187 (vs), 764 (m) cm^{-1}. Elem. Anal. Calcd for $C_{72}H_{80}N_8S_8Ag_4$: C, 49.54%; H, 4.62%; N, 6.42%. Found: C, 48.56%; H, 4.43%; N, 6.23%.

Synthesis of $Cu_6[CS_2(2,6\text{-}Me_2C_6H_3NC(H)=NC_6H_3Me_2)]_6$, 7. To a stirring solution of $Cu_2[(2,6\text{-}^iPr_2C_6H_3N)_2C(H)]_2$ (100 mg, 0.12 mmol) in THF (20 mL) was added excess CS_2. The reaction was allowed to stir overnight during which the solution changed from a yellow color to a dark orange. The solvent was removed under vacuum to yield an orange powder (91 mg, 43% yield). X-ray crystals were grown from a saturated chloroform/heptane solution at room temperature. ^1H NMR ($CDCl_3$, 500 MHz): δ 9.36 (s, 1H, CH), 7.34 (m, 1H, Ph), 7.17 (m, 1H, Ph), 6.99 (m, 3H, Ph), 2.66 (br, m, 2H, CH), 1.15 (br, m, 12H, Me), 1.0 (br, d, $^3J_{H-H}$ = 4.5 Hz. 12H, Me) ppm. ^{13}C NMR ($CDCl_3$, 125 MHz): δ 213 (quat), 150.8 (methine), 138.7 (Ph), 129.6 (Ph), 129.0 (Ph) 128.2 (Ph) 125.5 (Ph), 125.2 (Ph), 124.5 (Ph), 124.3 (Ph), 123.1 (Ph), 27.5 (methine), 25.5 (Me), 25.0 (Me), 24.0 (Me), 23.9 (Me) ppm. IR (KBr): 3060 (w), 2962 (m), 2921 (w), 2859 (w), 1650 (m), 1585 (w), 1376 (s, br), 1294 (m), 1254 (m), 1209 (m), 1127 (w), 1078 (w), 829 (s, br), 751 (w), 710 (w), 538 (m) cm^{-1}. Anal. Calcd for $C_{156}H_{210}N_{12}S_{12}Cu_6$: C, 62.05%; H, 7.01%; N, 5.57%. Found: C, 61.21%; H, 7.06%; N, 5.20%.

Table 1. X-ray Crystallographic Data for Complexes 1−5, 7, and 8

	1	2	3	4	5	7	8
CCDC deposit number	905800	982999	1010914	1010913	905801	1012827	1012891
empirical formula	$C_{34}H_{38}N_4Cu_2$	$C_{34}H_{38}N_4Ag_2$	$C_{50}H_{70}N_4Cu_2$	$C_{50}H_{70}N_4Ag_2\cdot 1.25CH_2Cl_2$	$C_{88}H_{80}N_8O_4S_8Cu_4$	$C_{158}H_{216}Cl_6N_{12}S_{12}Cu_6$	$C_{174}H_{262}N_{12}S_{12}Ag_6$
fw (g/mol)	629.76	718.42	854.18	1048.99	1824.24	3262.07	3553.88
cryst habit, color	prism, colorless	prism, colorless	prism, colorless	prism, colorless	prism, yellow	prism, orange	prism, orange
T (K)	110(2)	100(1)	100(2)	100(2)	100(2)	100(2)	100(2)
space group	$P\bar{1}$	$P\bar{1}$	$C2/c$	$C2/c$	$C2/c$	$P\bar{1}$	$Ia\bar{3}$
cryst syst	triclinic	triclinic	monoclinic	monoclinic	monoclinic	triclinic	cubic
V (Å^3)	738.9(6)	750.07(12)	9320.1(14)	10582.9(15)	8789.96	4100.3(2)	33644.8
a (Å)	7.346(4)	7.3909(7)	46.536(4)	42.914(3)	26.2634(6)	14.5584(5)	32.283(4)
b (Å)	9.567(5)	9.4593(9)	10.3918(9)	11.6524(9)	16.9911(4)	16.4788(5)	32.283(4)
c (Å)	11.152(6)	11.4957(11)	21.3697(18)	27.242(2)	23.3532(8)	20.3513(6)	32.283(4)
α (deg)	93.341(6)	78.9590(10)	90	90	90	99.567(2)	90
β (deg)	107.551(6)	72.0200(10)	115.5950(10)	129.0260(10)	122.492(1)	107.303(2)	90
γ (deg)	94.787(7)	85.2960(10)	90	90	90	112.091(2)	90
Z	1	1	8	8	4	1	8
calcd density (Mg/m^3)	1.415	1.590	1.217	1.317	1.326	1.321	1.403
abs coeff (mm^{-1})	1.469	1.335	0.949	0.902	1.152	3.569	0.888
final R indices [$I > 2\sigma(I)$]	R1 = 0.0457	R1 = 0.0141	R1 = 0.0500	R1 = 0.0335	R1 = 0.0464	R1 = 0.0634	R1 = 0.0435
	wR2 = 0.0923	wR2 = 0.0359	wR2 = 0.1207	wR2 = 0.0990	wR2 = 0.0910	wR2 = 0.1578	wR2 = 0.0957

Synthesis of $Ag_6[CS_2(2,6\text{-}Me_2C_6H_3NC(H)=NC_6H_3Me_2)]_6$, 8. To a stirred solution of **4** (500 mg, 5.3 mmol) in toluene (25 mL) was added an excess of carbon disulfide (~2 mL). The reaction was allowed to stir for 24 h during which time the color became a bright orange/red. To this resulting solution was added ~50 mL of methanol, and the mixture was stored at −20 °C overnight. The resulting crystalline material was collected on a fritted filter and washed with 5 mL of acetone (250 mg, 43%). X-ray quality crystals were grown from a saturated solution of THF at room temperature; however, other attempts were from chloroform/acetonitrile and result in solvent-containing structures. Hence, the elemental analysis contains solvent molecules, while the crystal structure deposited in the CCDC does not. ^{1}H NMR (CD_2Cl_2, 500 MHz): δ 9.39 (s, 1H, CH), 7.37 (t, 1H, $^3J_{H-H}$ = 7.5 Hz, Ph), 7.14 (d 1H, $^3J_{H-H}$ = 7.5 Hz, Ph), 7.06 (br s, 3H, Ph), 2.79 (sept, 1H, $^3J_{H-H}$ = 6.5 Hz, CH), 2.70 (sept, 1H, $^3J_{H-H}$ = 7 Hz, CH), 1.21 (br s, 6H, Me), 1.15 (br s, 6H, Me), 1.03 (d, 12H, $^3J_{H-H}$ = 6.5 Hz, Me) ppm. ^{13}C NMR (CD_2Cl_2, 125 MHz): δ 152.2 (Ph), 145.3 (Ph), 144.7 (Ph), 139.0 (Ph), 137.9 (Ph), 129.9 (Ph), 124.9 (Ph), 124.7 (Ph), 123.4 (Ph), 29.5 ($CH(CH_3)_2$), 27.7 ($CH(CH_3)_2$), 25.8 ($CH(CH_3)_2$), 24.3 ($CH(CH_3)_2$), 24.1 ($CH(CH_3)_2$) ppm. IR (KBr): 3062 (m), 3024 (w), 2961 (vs), 2927 (s), 2867 (s), 1939 (vs), 1588 (m), 1461 (s), 1382 (s), 1356 (s), 1293 (vs), 1253 (vs), 1220 (vs), 1173 (s), 1126 (m), 1100 (m), 1080 (m), 989 (m), 867 (s), 798 (m), 753 (m), 720 (m), 651 (w), 548 (w), 496 (w) cm^{-1}. Anal. Calcd for $C_{156}H_{210}N_{12}S_{12}Ag_6\cdot 4CHCl_3\cdot 4CH_3CN$: C, 51.38%; H, 5.80%; N, 5.71%. Found: C, 51.24%; H, 6.02%; N, 5.34%.

Computational Details. The experimental structure of $Cu_2[(2,6\text{-}Me_2C_6H_3N)_2C(H)]_2$, **1**, was calculated without simplification. The structures of **1** and $Cu_2[(2,6\text{-}Me_2C_6H_3N)_2C(H)]_2O_2$, **1-O$_2$**, were optimized in THF solvent using density functional theory (DFT). The excited states of **1** were calculated using time-dependent DFT (TDDFT) at its optimized structure. All DFT and TDDFT calculations were performed using the Gaussian 09 suite of ab initio programs[31] for a hybrid meta-GGA density functional ωB97X-D[32] in conjunction with all-electron 6-31+G(d) basis set for the H, C, N, and O atoms, and the Stuttgart relativistic effective core potential basis set for Cu {(ECP10MWB), (8s7p6d2f1g) → [6s5p3d2f1g]}. The ωB97X-D functional was selected for this study because it contains both long-range and dispersion corrections, which are important for the modeling of weak noncovalent interactions. The solvent effect was calculated using the integral equation formalism polarizable continuum model (IEFPCM)[33] with Truhlar and co-workers' SMD atomic radii.[34] An ultrafine integration grid (99,590) was used for numerical integrations. The ground state of the structure was confirmed through the calculation and comparison of its low-spin and high-spin analogs.

Crystal Structure Determination and Refinement. The selected single crystal of **1**−**5**, **7**, and **8** was mounted on nylon cryoloops using viscous hydrocarbon oil. X-ray data collection was performed at 100(2) K. The X-ray data were collected on a Bruker CCD diffractometer with monochromated Mo Kα radiation (λ = 0.710 73 Å). The data collection and processing utilized Bruker Apex2 suite of programs.[35] The structures were solved using direct methods and refined by full-matrix least-squares methods on F^2 using Bruker SHELEX-97 program.[36] All non-hydrogen atoms were refined with anisotropic displacement parameters. All hydrogen atoms were added on idealized positions and not allowed to vary. Thermal ellipsoid plots were prepared by using X-seed[37] with 30% or 50% of probability displacements for non-hydrogen atoms. Crystal data and details for data collection for complexes **1**−**5**, **7**, and **8** are also provided in Table 1.

RESULTS AND DISCUSSION

Synthesis and Spectroscopy. Reaction of $[Cu(NCMe)_4]$-PF_6 or AgO_2CCH_3 with M[(2,6-$R_2C_6H_3N$)C(H)], M = Na or NEt_3H, yields the dinuclear complexes, $M_2[(2,6\text{-}R_2C_6H_3N)C(H)]_2$, M = Cu, **1**, R = Me; M = Ag, **2**, R = Me; M = Cu, R = ^{i}Pr, **3**; M = Ag, R = ^{i}Pr, **4**, eq 1. Silver acetate was used as a starting material since the byproduct, triethylammonium acetate, is a liquid and can be easily separated from the reaction mixture. Further, salt metathesis reactions using $AgNO_3$ led to intractable mixtures and formation of a black precipitate, possibly Ag_2O. Complex **1** is slightly air- and moisture-sensitive, but indefinitely stable when stored under an inert atmosphere. It has good solubility in THF and chloroform, being slightly less soluble in arene solvents, and sparingly soluble in aliphatic solvents. The silver analog, **2**, has negligible solubility in arene solvents and is sparingly soluble in THF, but displays good solubility in chloroform. Complexes **2**

dx.doi.org/10.1021/ic501694d | Inorg. Chem. 2014, 53, 11357−11366

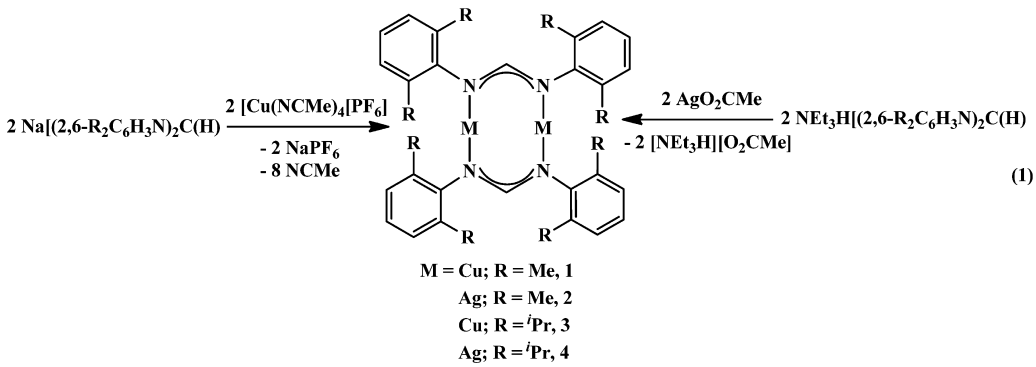

(1)

and **4** exhibit moderate light-sensitivity in solution but can be left indefinitely as a solid without decomposition, but **1** and **3** are not sensitive in either phase.

The ^{1}H NMR spectra of **1** and **2** show symmetric ligand environments and the methyl resonance at 2.57 and 2.34 ppm, respectively, and the formamidinate proton located at 6.86 and 7.28 ppm, respectively. Interestingly, the ^{1}H NMR spectrum of **3** revealed two distinct methyl groups for each isopropyl group, and heating **3** to 70 °C in $CDCl_3$ did not lead to coalescence of the resonances. For **4**, two ^{i}Pr groups at 1.17 and 1.19 ppm were also observed. We attribute the multiple signals for **3** and **4** to steric crowding, which restricts the motion on the NMR time scale and therefore leads to different signals. For **2** and **4**, an apparent triplet of doublets is observed for the formamidinate backbone proton, with coupling constants of 16.2 and 17 Hz, respectively, arising from coupling of the proton to ^{107}Ag, ^{109}Ag, and ^{107,109}Ag. Unfortunately, no signal was observed in the ^{107,109}Ag NMR spectrum.[38] More Ag−H coupling was observed in complex **4** than **2**, which could be due to the influence of several factors, including solvent. Complex **2** has limited solubility in toluene; therefore, its ^{1}H NMR spectrum was performed in $CDCl_3$. However, increased rigidity of the complex could be responsible for the Ag−H coupling as well, with less fluxional behavior in solution with **4** than **2**.

Since reactions of dinuclear Ag(I) amidinates with CS_2 that form dithiocarbamates have not been well-characterized, we examined this reactivity. Upon addition of CS_2 to complexes **1**−**4**, yellow solutions were obtained, indicating that the reaction had occurred. Reactions of the silver complexes **2** and **4** with CS_2 in THF rapidly produced a black precipitate which we presume to be Ag_2S. However, when the reactions were performed in toluene or $CHCl_3$, little to no precipitate is observed, and a yellow solution persists. The ^{1}H NMR spectra showed asymmetric ligand environments with two distinct, chemically inequivalent methyl groups: 2.06 and 2.20 ppm for **5** and 2.17 and 2.04 ppm for **6**. Additionally, resonances at 9.42 and 9.46 ppm can be attributed to the formamidinate proton on the backbone of a localized imine for **5** and **6**, respectively. Interestingly, the reaction of CS_2 with the dinuclear Cu(I) β-diiminato complex does not lead to insertion but rather activation of the CS_2.[39] We note that reactions with substrates having hard donor atoms such as CO_2 and PhNCO do not react, demonstrating the propensity of group 11 metals for soft donor atoms such as sulfur.

While reactions of **1** and **2** with CS_2 are nearly instantaneous, reactions with **3** and **4** using the same solvent and under identical conditions are slower, but do produce orange solutions over time. After 4 h, the ^{1}H NMR spectrum of **3** with CS_2 yielded only **3** but after 12 h a new product is observed. As with **5** and **6**, the ^{1}H NMR spectra of the products showed the formamidinate proton at 9.36 and 9.39 ppm for **7** and **8**, respectively.

X-ray Crystallography Analysis. The structures of complexes **1**−**4** show an inversion center through the midpoint of the M−M interaction. The metrical parameters for the Cu species, **1** and **3**, as well as the Ag compounds, **2** and **4**, are nearly identical. The Cu1−N1 and Cu1−N2* bond distances of 1.872(3) and 1.870(3) Å, respectively, in **1**, Figure 1, are similar to the 1.869(1) Å in $Cu_2[^i$PrNC(Me)NiPr$]_2$.[12] However, the 2.548(1) Å Cu−Cu distance in **1** is nearly 0.15 Å longer than the 2.414(1) Å in $Cu_2[^i$PrNC(Me)NiPr$]_2$.[12]

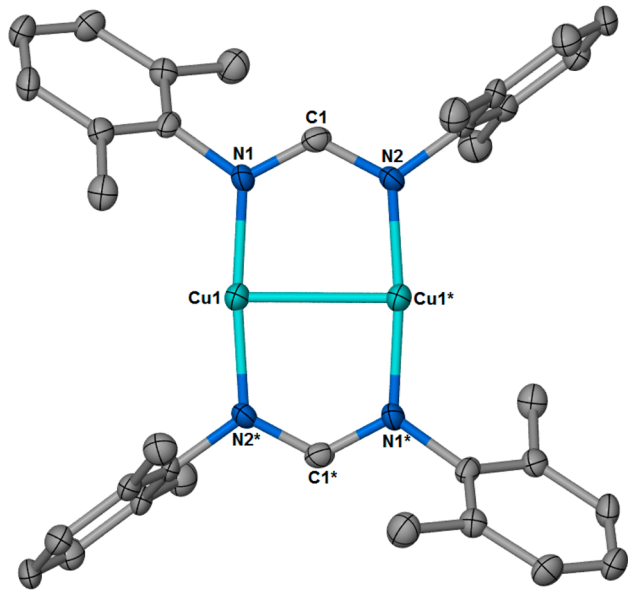

Figure 1. Thermal ellipsoid plot of **1** shown at the 50% probability level. Hydrogen atoms have been omitted for clarity. Selected bond distances and angles: Cu1−N1, 1.872(4) Å; Cu1−N2, 1.870(4) Å; Cu1−Cu1*, 2.548(1) Å; N1−Cu1−N2, 173.7(1)°; N1−Cu1−Cu1*, 86.34(10)°.

The structure of **2** revealed identical connectivity and symmetry to **1**, Figure 2. The Ag−Ag bond distance of 2.7527(3) Å in **2** and Ag−N distances of 2.0980(12) and 2.1077(12) Å are nearly identical to those in $Ag_2[(2\text{-}OCH_3C_6H_4N)_2C(H)]_2$,[16] 2.7801(7) Å, and 2.104(5) and 2.123(5) Å, respectively. Due to the larger size of Ag(I) than Cu(I),[40] the angle of N1−Ag1−Ag1* is more acute, 84.20(3)°, compared to the N2−Cu1−Cu1* angle of 86.34(10)°, indicating more buckling in the amidinate chelate. Both **1** and **2** have delocalized amidinate ligands based on their N−C−

dx.doi.org/10.1021/ic501694d | Inorg. Chem. 2014, 53, 11357−11366

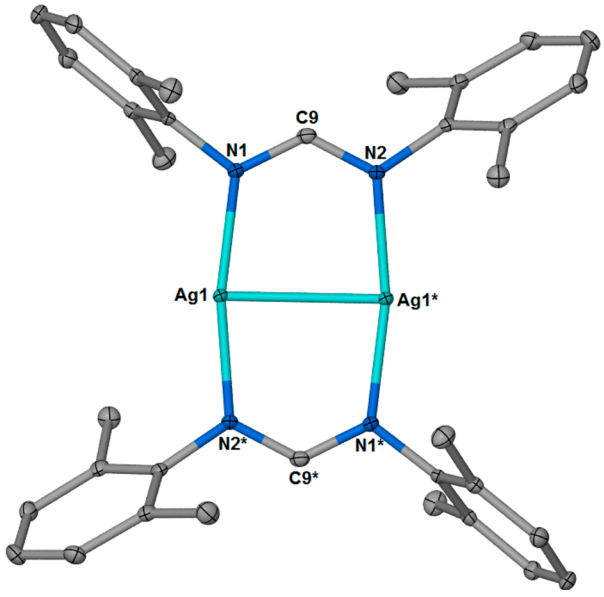

Figure 2. Thermal ellipsoid plot of **2** shown at the 50% probability level. Hydrogen atoms have been omitted for clarity. Selected bond distances and angles: Ag1−N1, 2.0980(12) Å; Ag1−N2*, 2.1077(12) Å; Ag1−Ag1*, 2.7527(3) Å; N1−Ag1−N2*, 168.89(5)°; N1−Ag1−Ag1*, 84.20(3)°.

N bond lengths in the backbone, 1.308(5) and 1.338(5) Å in **1** and 1.3164(1) and 1.3212(1) Å in **2**. In all cases, complexes **1**−**4** display metal−metal bond distances that are shorter than the sum of their van der Waals radii: 1.40 and 1.72 Å for Cu and Ag, respectively.[41]

The isopropyl derivatives, $M_2[(2,6\text{-}^iPr_2C_6H_3N)_2C(H)]_2$, M = Cu, **3**; Ag, **4**, were also found to be dinuclear in the solid-state, Figures 3 and 4, similar to guanidinate complexes with 2,6-diisopropylphenyl substituents, $Cu_2[2,6\text{-}^iPr_2C_6H_3N)_2C(NMe_2)]_2$.[42]

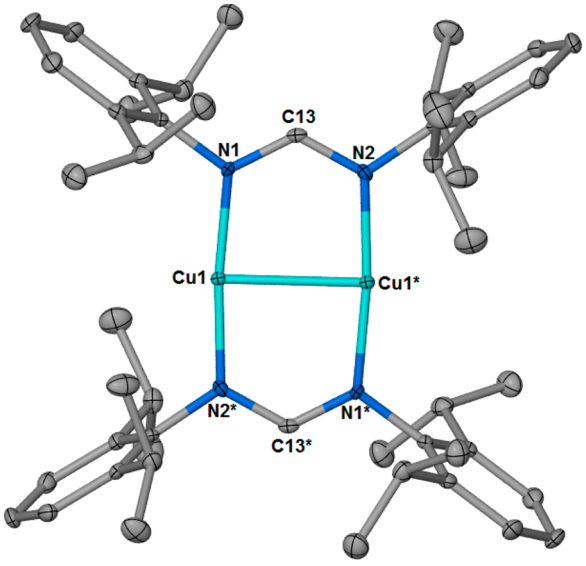

Figure 3. Thermal ellipsoid plot of **3** shown at the 50% probability level. Hydrogen atoms have been omitted for clarity. Selected bond distances and angles: Cu1−N1, 1.880(2) Å; Cu1−N2*, 1.879(2) Å; Cu1−Cu1*, 2.5420(7) Å; N1−Cu1−N2*, 173.73(10)°; N1−Cu1−Cu1*, 86.29(7)°.

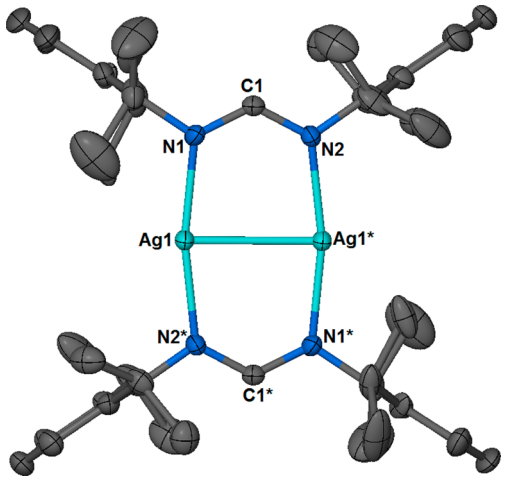

Figure 4. Thermal ellipsoid plot of **4** shown at the 50% probability level. Hydrogen atoms and solvent molecules have been omitted for clarity. Ag1−N1, 2.110(3) Å; Ag1−N2*, 2.111(3) Å; Ag1−Ag1*, 2.7544(6) Å; N1−Ag1−N2*, 168.88(11)°; N1−Ag1−Ag1*, 83.68(8)°.

The structure of **5** consists of a tetranuclear copper(I) complex, where each copper coordinates to three different sulfur donors, from $-CS_2$ bridging ligands, in trigonal geometry, Figure 5. The four disulfide ligands are formamidines modified into dithiocarbamates, each showing an appended CS_2 moiety on one nitrogen. The complex core, consisting of four copper(I) atoms, displays a tetrahedral arrangement where each trigonal face is capped by a dithiocarbamate in a $\kappa^{1-2}S$ and κ^3S coordination way. The metal atoms are located at 0.1365(11) and 0.0747(12) Å out of the S−S−S plane. Each disulfide ligand binds $\kappa^{1-2}S$ and κ^3S to three copper units (one sulfur atom bonded to two coppers and one bonded to only one). Despite the different bonding ways, copper−sulfur bond lengths differ little from the average 2.254 Å with a range from 2.227 to 2.291(2) Å, Table 2. The copper−copper lengths are fairly short, and they are influenced by the way in which sulfur is bonded: those copper(I) atoms bounded to the same sulfur donor ($\kappa^{1-2}S$) exhibit shorter metal−metal distances (2.630(2) and 2.6405(18) Å) than the ones bridged by different sulfur atoms from the same CS_2 unit (2.784(3) and 2.884(3) Å). The average bond angle Cu−Cu—Cu is 60°, corresponding to a tetrahedron, which ranges from 56.77° to 66.35°, Figure 5. This copper tetramer is closely related to formerly reported molecules with S−C−S bridging ligands.[43] The tetrakis(μ_3-*N*,*N*-di-*n*-butyldithiocarbamato-S,S,S′)-tetra-copper(I) complex[44] obtained from the comproportionation reaction of activated Cu powder with $Cu(S_2CNBu_2)_2$ possesses four bridging S_2-C-NR_2 ligands. The tetrakis(*p*-tolyldithio-carboxylato-S,S,S′)-copper(I)[45] has four S_2-C-tol bridging ligands, while tetrakis((μ_3-2,6-di-*tert*-butyl-4-methylphenoxy) thioxanthato)-copper(I))[46] has four S_2-C-O-Ar bridging ligands. In all of the forementioned structures, each copper has a trigonal planar coordination and is positioned slightly out of the S−S−S plane, as in compound **5**. This complex resembles the active center of the cytochrome *c* oxidase, where two copper atoms are bound to the same sulfur donor.

The silver analog proved to be more difficult to isolate. Similar to the reaction to yield **5**, the solution turned from colorless to yellow but was significantly less soluble in organic solvents. The ^1H NMR spectrum yielded a single product;

dx.doi.org/10.1021/ic501694d | *Inorg. Chem.* 2014, 53, 11357−11366

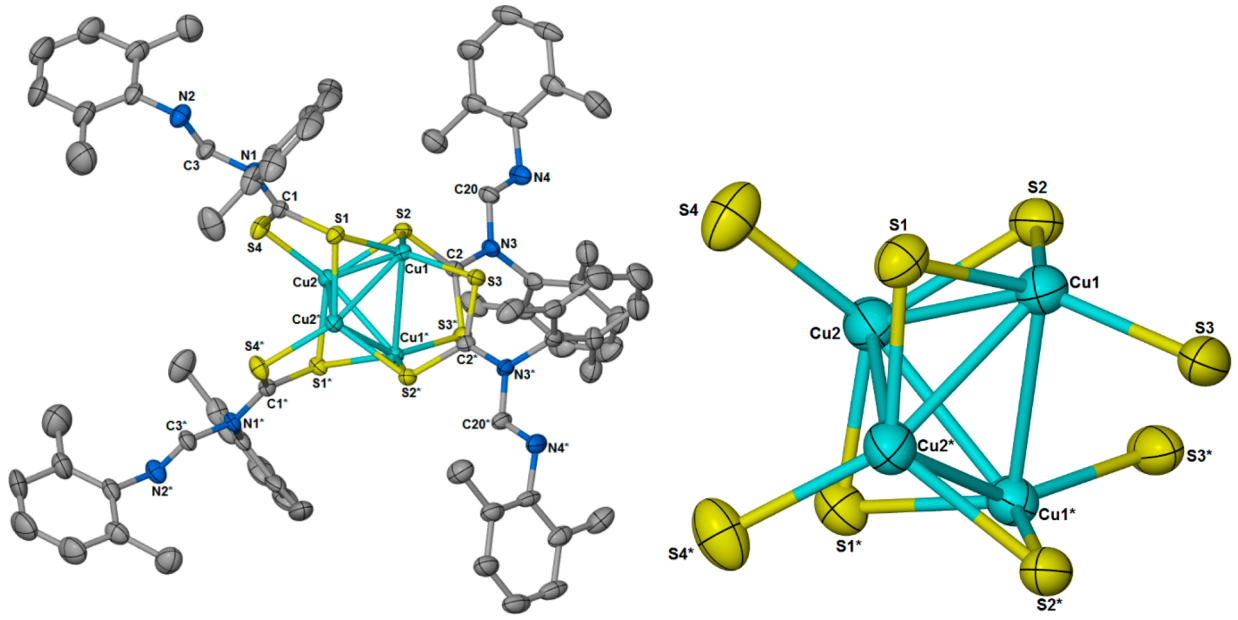

Figure 5. (Left) Thermal ellipsoid of **5** shown at the 30% probability level with the hydrogen atoms and solvent molecules removed for clarity. (Right) Cu_4S_8 core of **5** shown at the 50% probability level with all other atoms deleted.

Table 2. Selected Bond Distances (Å) and Angles (deg) of 5

bond distance (Å)/angle (deg)	5
Cu1−S1, Cu1*−S1*	2.243(2)
Cu1−S2, Cu1*−S2*	2.261(3)
Cu1−S3, Cu1*−S3*	2.227(2)
Cu2−S1, Cu2*−S1*	2.256(3)
Cu2−S2, Cu2−S2*	2.291(2)
Cu2−S4, Cu2*−S4*	2.245(2)
Cu1−Cu2	2.641(2)
Cu1−Cu1*	2.785(3)
Cu1−Cu2*	2.630(3)
Cu2−Cu2*	2.884(2)
N1−C3, N1*−C3*	1.388(9)
C3−N2, C3*−N2*	1.235(7)
N3−C20, N3*−C20*	1.38(1)
C20−N4, C20*-N4*	1.24(1)
S1−C1−S4, S1*−C1*−S4*	124.9(4)
S2−C2−S3, S2*−C2*−S3*	122.0(5)

however, the mixture becomes insoluble over time, which we attribute to the formation of a polymeric structure. Further, the Au analog has been isolated as a polymer with repeating dinuclear units, $\{Au_2[CS_2(2,6\text{-}Me_2C_6H_3NC(H)=N\text{-}C_6H_3Me_2)]_2\}_n$, that are bridged by aurophilic interactions.[47]

Reaction of **3** and **4** with CS_2 yields $M_6[CS_2(2,6\text{-}^iPr_2C_6H_3\text{-}NC(H)=NC_6H_3{}^iPr_2)]_6$, M = Cu, **7**, Figure 6; Ag, **8**, Figure 7, and crystallizes as a hexameric cluster with a M_6S_{12} core. Interestingly, with the dimethylphenyl-derivative, a tetranuclear cluster is obtained with Cu, but hexanuclear cores were isolated with diisopropylphenyl. Each M(I) metal is coordinated to three sulfur atoms in an $\kappa^1,\kappa^1,\kappa^1$-S fashion with Cu1−S bond distances of 2.2198(13), 2.2285(15), and 2.2425(14) Å in **7** and all Ag−S bond distances of 2.5008(2), 2.4779(3), and 2.4779(3) Å, Table 3, since **8** has a 6-fold axis of symmetry. One sulfur in each dithiocarbamate ligand is bound η^1 while the other is μ_2,η^2-S between two metal centers. The Cu−Cu bond distances in **7** are similar to those observed in **5**. It is worth noting that while several dithiocarbamate clusters of Cu(I)[44−46,48−50] and Ag(I)[51−55] are known, none are from CS_2 insertion or derived from a dinuclear species.

Electronic Absorption and Luminescence Spectroscopy. Absorbance spectra for solutions of the dinuclear Cu(I) and Ag(I) amidinate complexes, **1**−**4**, prepared in THF, displayed absorbance maxima at 255 nm, Figure 8, with the Cu(I) and Ag(I) complexes displaying fwhm of ca. 6500 cm^{-1}. The amidinate complexes are relatively good chromophores in the UV region. For example, **1** shows an extinction coefficient of 20 650 M^{-1} cm^{-1} at 255 nm. Upon addition of CS_2 to the dinuclear complexes, yellow or orange solutions were obtained, giving rise to new structured spectral features which are red-shifted relative to the original band. For instance, as shown in the inset of Figure 8, the difference spectrum resulting from subtracting the extinction spectrum of **1** from **5** is bimodal and spans the region from 265 to 450 nm, with transitions centered near 295 and 340 nm.

Solutions of both **1** and **5** displayed green emission when excited in the UV, although the latter showed much weaker luminescence, Figure 9. Complexes **1** and **5** show similarly large emission Stokes shifts of ca. 20 500 cm^{-1}, compared to typical values of 1000−4000 cm^{-1} for organic dyes. On the other hand, no luminescence signal above the solvent blank was discernible for the Ag(I) analogs of the Cu(I) amidinate complexes nor was any observed with **3**, Figure 9. Emission wavelength-dependent excitation spectra of **1** dissolved in THF when the emission was monitored at 535 nm (peak) and 630 nm (red edge) were essentially superimposable (data not shown). This suggests a lack of ground-state heterogeneity (e.g., association, aggregation, or multiple emitting species), which would give rise to distinct differences in the scans. Figure 9 also presents normalized excitation wavelength-dependent emission scans for **1** in THF. Again, the fact that these spectra overlay one another reveals a well-behaved photophysical system with no discernible red-edge effect.[56]

Luminescence quantum yields (φ) for **1** and **5** were determined relative to an optically dilute reference lumino-

dx.doi.org/10.1021/ic501694d | Inorg. Chem. 2014, 53, 11357−11366

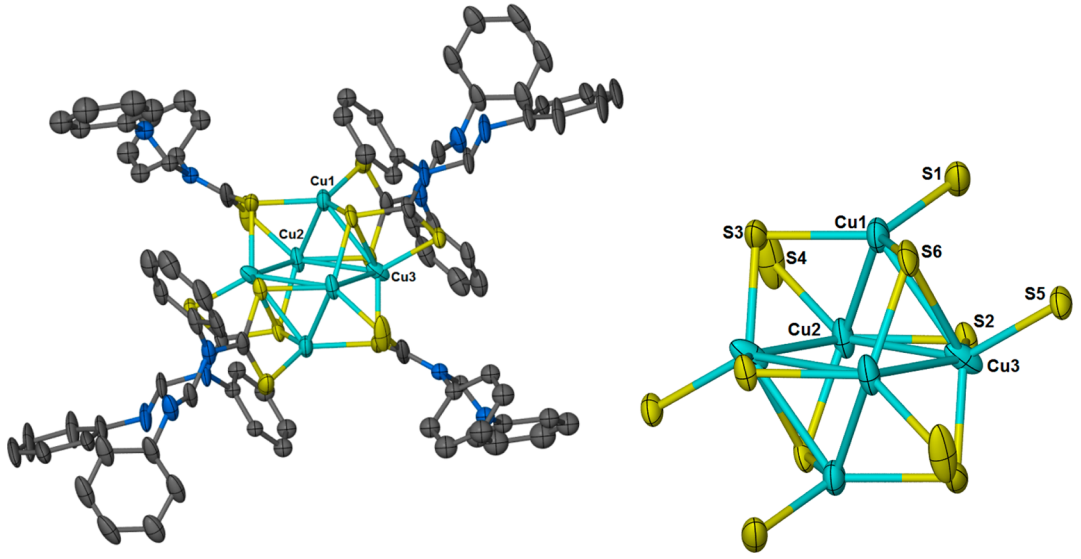

Figure 6. (Left) Thermal ellipsoid of **7** shown at the 50% probability level with the isopropyl groups, hydrogen atoms and solvent molecules removed for clarity. (Right) Cu_6S_{12} core of **7** shown at the 50% probability level.

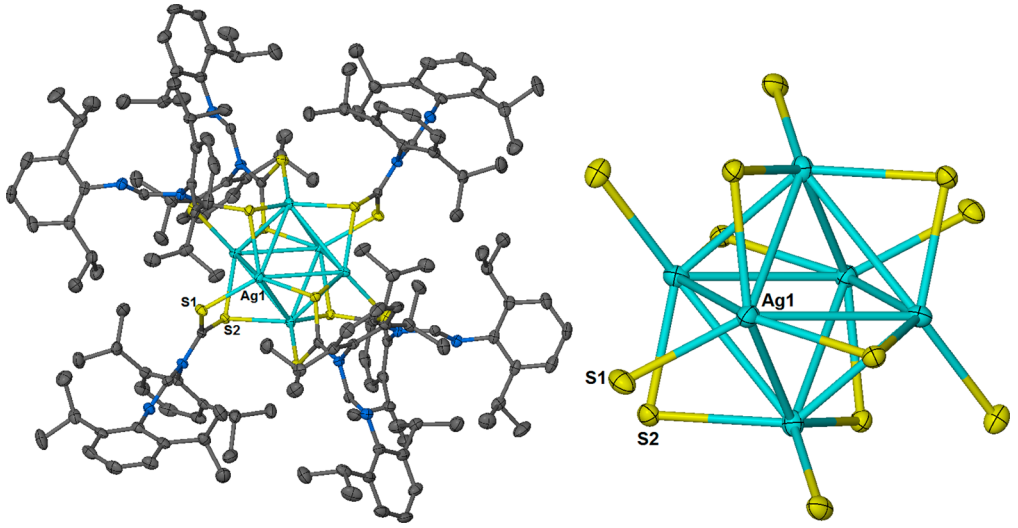

Figure 7. (Left) Thermal ellipsoid of **8** shown at the 50% probability level with the hydrogen atoms and solvent molecules removed for clarity. (Right) Ag_6S_{12} core of **8** shown at the 50% probability level.

Table 3. Selected Bond Distances (Å) and Angles (deg) of 7 and 8

bond distance (Å)/angle (deg)	7	8
M1−S1	2.2285(15)	2.5008(2)
M1−S2	2.2198(13)	2.4779(3)
M1−M1	2.6921(11)	3.0001(3)
M1−M1′	2.7351(11)	3.3178(3)
M1−M1−M1 (apical)	68.09(3)	60.000(5)
M1−M1−M1 (apical)	56.63(2)	56.430(6)
M1−M−M (meridinal)	71.55(3)	90.00(1)

phore solution of quinine sulfate in 0.1 M H_2SO_4 ($\varphi_{ref} = 0.577$) at 350 nm excitation using

$$\phi_S = \phi_{ref} \frac{L_S}{L_{ref}} \frac{OD_{ref}}{OD_S} \frac{{n_S}^2}{{n_{ref}}^2} \quad (2)$$

In eq 2, L represents the total, integrated luminescence intensity at the excitation wavelength, OD is the optical density

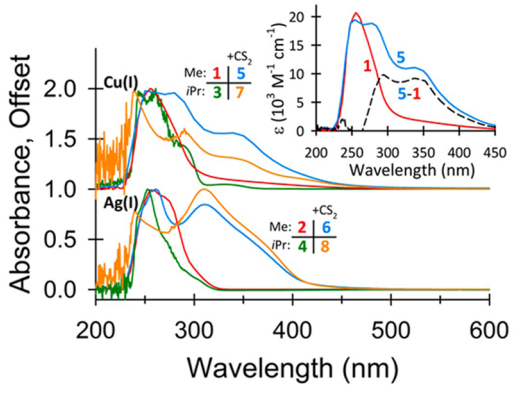

Figure 8. Normalized absorbance spectra for 10^{-4} M dinuclear Cu(I) and Ag(I) complexes in argon-purged THF (solid lines). Note that spectra are offset vertically for ease of visualization. Inset: Extinction spectra for the Cu(I) complexes **1** and **5** and the difference spectrum (dashed profile).

dx.doi.org/10.1021/ic501694d | *Inorg. Chem.* 2014, 53, 11357−11366

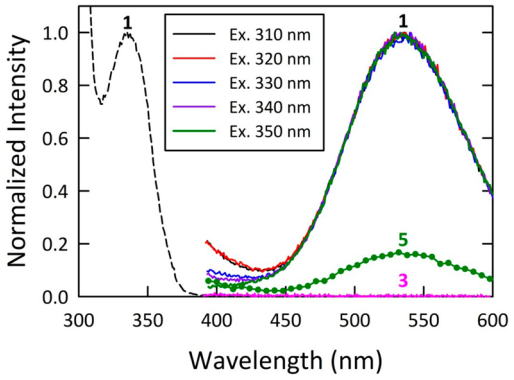

Figure 9. Emission spectra of **1** and **3** (10^{-4} M in degassed THF) for various excitation wavelengths. Shown for comparison is the emission spectrum of the same molar concentration of **5** in THF, excited at 350 nm. The associated excitation spectrum of **1**, monitored at 535 nm, is shown as the broken profile.

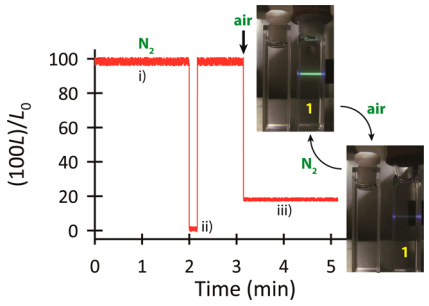

Figure 10. Temporal response profile of luminescence (ex: 350 nm, em: 535 nm) from 10^{-4} M **1** in THF (L and L_0 are defined in eq 2). Segments labeled i, ii, and iii denote conditions under which the sample was sparged with nitrogen, the instrument detection shutter was closed, and signal following exposure of the solution to ambient conditions, respectively. The arrow indicates the time at which the sample was exposed to laboratory air, followed by replacement of the sample in the sample chamber. Not shown explicitly in this trace is an 8−10 s window of dead time during which the sample was exposed to air and manually mixed. Within the time required to achieve this task, the sample had already achieved steady-state conditions. In the photographs shown, the left cuvette reference contains only THF and the cuvette on the right contains **1** in THF. Both cuvettes are irradiated from the right-hand side with 342 nm light from a HeCd laser.

at the same excitation wavelength, and n is the refractive index of the solvent used. The subscripts S and ref denote the sample (unknown) and reference, respectively. Luminescence quantum yields of 0.85×10^{-2} and 6.32×10^{-4} were determined for **1** and **5**, respectively, both measured in deoxygenated THF.

With the luminescent Cu(I) cluster **1** in hand, we considered whether it might possess a long-lived excited state, making it a suitable molecular probe for luminescence-based oxygen sensing. Collisional quenching by oxygen in a homogeneous medium can be described by the Stern−Volmer equation, eq 3[57]

$$\frac{L_0}{L} = 1 + K_{SV} pO_2 \tag{3}$$

where L_0 and L are the luminescence intensities in the absence and presence of O_2, K_{SV} is the Stern−Volmer quenching constant, and pO_2 is the partial pressure of O_2. Indeed, as shown in Figure 10, exposure of a nitrogen-saturated THF solution of **1** to laboratory air results in a rapid and nearly 6-fold drop in the observed luminescence intensity. The response is essentially instantaneous. In the few seconds required to remove the septum, recap the cuvette and invert twice, and place back in the sample chamber, quenching was already observed and a steady state achieved. Assuming linear Stern−Volmer behavior, in terms of K_{SV}, this amount of quenching upon going from nitrogen to air amounts to a sensitivity of 0.2337 kPa^{-1}. Interestingly, when the sample is sparged with nitrogen and reanalyzed, the fluorescence returned (see Supporting Information Figure S1), indicating the reversibility of quenching by O_2. By comparison, the benchmark O_2-sensing dye tris(4,7′-diphenyl-1,10′-phenanthroline)ruthenium(II), $[Ru(dpp)_3]^{2+}$, sequestered in sol−gel-derived silica films showed K_{SV} values an order of magnitude smaller, ranging from 0.0234 to 0.0545 kPa^{-1} and monotonically increasing as the curing temperature was increased from ambient temperature to 300 °C.[46] In fact, quenchometric O_2 sensors that have employed $[Ru(dpp)_3]^{2+}$ as the luminophore have typically reported L_0/L_{min} sensitivities in the 3−7 range (L_{min} denotes the signal arising from 100% oxygen) whereas our system suggests a sensitivity in terms of L_0/L_{min} close to 25. Similarly high values based on $[Ru(dpp)_3]^{2+}$ have only been observed previously for media with high oxygen diffusivity, such as perfluoroalkyl organically modified silicates (ORMOSILs) or RTV-118 silicone.[58] Although luminescent lifetimes were not determined in this work, this high sensitivity to oxygen implies a long-lived excited state, likely on the order of tens of microseconds or longer.

O_2 Quenching. To gain an understanding of the excited-state interaction between **1** and O_2, DFT and TDDFT calculations were performed. Complex **1** was fully optimized from its crystal structure coordinates, Figure S2 in the Supporting Information, and the ground state was found to be a singlet. The TDDFT calculated singlet and triplet excited states of **1** and the corresponding oscillator strengths are listed in Table S1 in the Supporting Information. The calculated oscillator strengths indicate that the absorption peak of **1** is around 255 nm, which matches well with the observed absorption spectra of **1** in THF. Since the transitions from singlet to triplet and higher order multiplet excited states are forbidden, the oscillator strengths of singlet−triplet transitions are not listed in Supporting Information Table S1. Even if some of these forbidden transitions gain intensity by spin−orbit splitting, their intensities in the absorption spectrum should still be very weak relative to the transitions to the singlet excited states.

Figure 11 shows the optimized structures of the triplet (**1-O_2-T**) and singlet (**1-O_2-S**) states of **1-O_2**. The calculated electronic energy of **1-O_2-T** is 31.62 kcal/mol, lower than that of **1-O_2-S**, which indicates that the ground state of **1-O_2** is a triplet. As shown in Figure 11, the O_2 molecule in **1-O_2-T** is about 5 Å away from the copper center. All optimization attempts to form Cu−O bonds at the triplet states failed. Such large distance means there is no interaction between **1** and O_2 at the ground state of **1-O_2**. The triplet electronic state of **1-O_2-T** is from the triplet ground state of O_2. Therefore, addition of O_2 into the solvent will not influence the absorption spectrum of **1**. However, once the photon was absorbed by **1-O_2-T**, the O_2 molecule will react with **1** and convert the spin-state of **1-O_2** from triplet to singlet with the formation of two strong Cu−O bonds of 2.076 and 2.057 Å, respectively. **1-O_2-S** also has slightly stretched O−O distance of 1.298 Å and a slightly

dx.doi.org/10.1021/ic501694d | Inorg. Chem. 2014, 53, 11357−11366

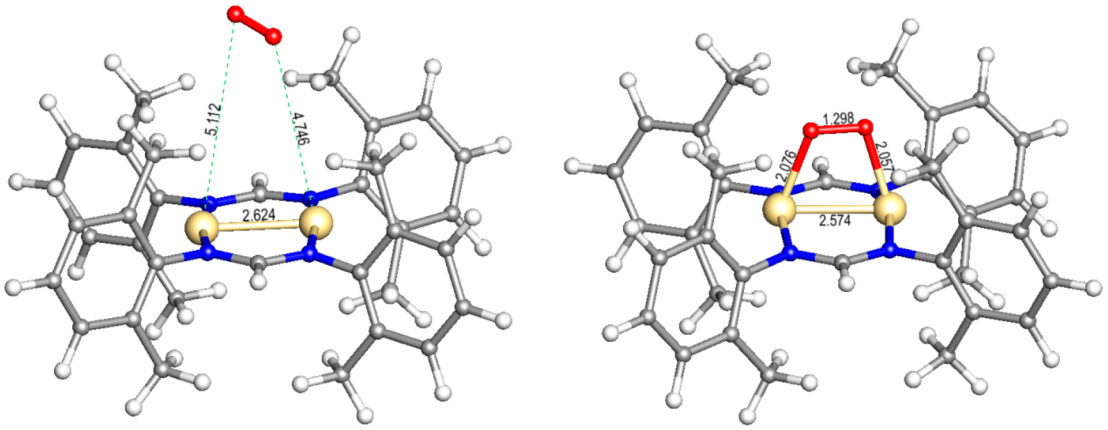

1-O_2-T **1-O_2-S**

Figure 11. Optimized triplet and singlet state structures of **1-O_2**. Bond lengths are in Å.

shortened Cu−Cu distance of 2.574 Å. Such strong interaction between O_2 and the copper atoms will change the electronic structure and transition properties of **1** significantly, and therefore change the observed emission spectra. This interaction explains why the addition of O_2 did not affect the absorption spectra, but changed the emission spectra of **1**.

CONCLUSION

We have synthesized and characterized new group 11 amidinate complexes, $M_2[(2,6\text{-}R_2C_6H_3N)_2C(H)]$, M = Cu, Ag; R = Me, ^{i}Pr, using ^{1}H and ^{13}C NMR, IR, UV−vis, and luminescence spectroscopy, and determined their structures by X-ray crystallography. The reactivity was examined with CS_2, with insertion observed into Cu−N bonds in **1** and **3** as well as the Ag−N bonds in **2** and **4**. With the dimethylphenyl substituted amidinate ligands, the copper complex yielded a tetranuclear cluster while the silver was presumably polymeric in nature. For the diisopropylphenyl derivatives, hexanuclear clusters were isolated with both copper and silver. Complex **1** was also shown to luminesce in the green region with a quantum yield of 0.85%, while **5** only showed a 0.06% quantum yield. Oxygen quenching was observed for **1**, and the basis of this was examined using DFT calculations which established that an excited triplet state of **1** interacts with O_2 which leads to the subsequent loss of singlet O_2. The high susceptibility of **1** to oxygen quenching suggests potential of this complex in luminescence-based O_2 sensors. In the future, our interest is to show cooperative chemistry between the two metal centers as well as to compare the electronic structure and reactivity of group 11 amidinate complexes.

ASSOCIATED CONTENT

Supporting Information

Optimized structure of **1**, O_2 quenching, and crystallographic details for **1**−**5**, **7**, and **8**. This material is available free of charge via the Internet at http://pubs.acs.org.

AUTHOR INFORMATION

Corresponding Author

*E-mail: walenskyj@missouri.edu.

Notes

The authors declare no competing financial interest.

ACKNOWLEDGMENTS

We gratefully acknowledge the Welch Foundation Grant A-0960 (J.P.F.), the University of Missouri—Columbia College of Arts & Science Alumni Association Faculty Incentive Award (J.R.W.), the National Natural Science Foundation of China (21373228), and the 100-Talent Program of Chinese Academy of Sciences (X.Y.) for funding. A.C.L. was supported by a Howard Hughes Medical Institute Fellowship through the University of Missouri—Columbia.

REFERENCES

(1) Serpe, A.; Artizzu, F.; Marchiò, L.; Mercuri, M. L.; Pilia, L.; Deplano, P. *Cryst. Growth Des.* **2011**, *11*, 1278.
(2) Merz, K. M.; Hoffmann, R. *Inorg. Chem.* **1988**, *27*, 2120.
(3) Fu, W.-F.; Gan, X.; Che, C.-M.; Cao, Q.-Y.; Zhou, Z.-Y.; Zhu, N. N.-Y. *Chem.—Eur. J.* **2004**, *10*, 2228.
(4) Zhang, J.-X.; He, J.; Yin, Y.-G.; Hu, M.-H.; Li, D.; Huang, X.-C. *Inorg. Chem.* **2008**, *47*, 3471.
(5) Ni, W.-X.; Qiu, Y.-M.; Li, M.; Zheng, J.; Sun, R. W.-Y.; Zhan, S.-Z.; Ng, S. W.; Li, D. *J. Am. Chem. Soc.* **2014**, *136*, 9532.
(6) Schmidbaur, H. *Gold Bull.* **2000**, *33*, 3.
(7) Pyykkö, P. *Chem. Rev.* **1997**, *97*, 597.
(8) Pyykkö, P. *Angew. Chem., Int. Ed.* **2004**, *43*, 4412.
(9) Blackburn, N. J.; Barr, M. E.; Woodruff, W. H.; van der Ooost, J.; de Vries, S. *Biochemistry* **1994**, *33*, 10401.
(10) Cotton, F. A.; Feng, X.; Matusz, M.; Poli, R. *J. Am. Chem. Soc.* **1988**, *110*, 7077.
(11) Shibayama, K.; Seidel, S. W.; Novak, B. M. *Macromolecules* **1997**, *30*, 3159.
(12) Lim, B. S.; Rahtu, A.; Park, J.-S.; Gordon, R. G. *Inorg. Chem.* **2003**, *42*, 7951.
(13) Jones, C.; Schulten, C.; Fohlmeister, L.; Stasch, A.; Murray, K. S.; Moubaraki, B.; Kohl, S.; Ertem, M. Z.; Gagliardi, L.; Cramer, C. J. *Chem.—Eur. J.* **2011**, *17*, 1294.
(14) Abdou, H.; Mohamed, A.; Fackler, J., Jr. *J. Cluster Sci.* **2007**, *18*, 630.
(15) Abdou, H. E.; Mohamed, A. A.; Fackler, J. P., Jr. *Inorg. Chem.* **2005**, *44*, 166.
(16) Abdou, H. E.; Mohamed, A. A.; Fackler, J. P., Jr. *Inorg. Chem.* **2007**, *46*, 9692.
(17) Abdou, H. E.; Mohamed, A. A.; Fackler, J. P. *Inorg. Chem.* **2007**, *46*, 9692.
(18) Abdou, H. E.; Mohamed, A. A.; Lopez-de-Luzuriaga, J. M.; Fackler, J. P., Jr. *J. Cluster Sci.* **2004**, *15*, 397.
(19) Abdou, H. E.; Mohamed, A. A.; López-de-Luzuriaga, J. M.; Monge, M.; Fackler, J. P. *Inorg. Chem.* **2012**, *51*, 2010.

(20) Mohamed, A. A. *Coord. Chem. Rev.* **2010**, *254*, 1918.
(21) Mohamed, A. A.; Abdou, H. E.; Irwin, M. D.; Lopez-de-Luzuriaga, J. M.; Fackler, J. P., Jr. *J. Cluster Sci.* **2003**, *14*, 253.
(22) Jiang, X.; Bollinger, J. C.; Baik, M.-H.; Lee, D. *Chem. Commun.* **2005**, 1043.
(23) Jiang, X.; Bollinger, J. C.; Lee, D. *J. Am. Chem. Soc.* **2005**, *127*, 15678.
(24) Archibald, S.; Alcock, N.; Busch, D.; Whitcomb, D. *J. Cluster Sci.* **2000**, *11*, 261.
(25) Barker, J.; Kilner, M. *Coord. Chem. Rev.* **1994**, *133*, 219.
(26) Radak, S.; Ni, Y.; Xu, G.; Shaffer, K. L.; Ren, T. *Inorg. Chim. Acta* **2001**, *321*, 200.
(27) Archibald, S. J.; Alcock, N. W.; Busch, D. H.; Whitcomb, D. R. *Inorg. Chem.* **1999**, *38*, 5571.
(28) Ren, T.; Lin, C.; Amalberti, P.; Macikenas, D.; Protasiewicz, J. D.; Clayton Baum, J.; L. Gibson, T. *Inorg. Chem. Commun.* **1998**, *1*, 23.
(29) Grohmann, A.; Schmidbaur, H. In *Comprehensive Organometallic Chemistry II*; Abel, E. W., Stone, F. G. A., Wilkinson, G., Eds.; Elsevier: Oxford, 1995; p 1.
(30) Roberts, R. M. *J. Org. Chem.* **1949**, *14*, 277.
(31) Frisch, M. J.; Trucks, G. W.; Schlegel, H. B.; Scuseria, G. E.; Robb, M. A.; Cheeseman, J. R.; Scalmani, G.; Barone, V.; Mennucci, B.; Petersson, G. A.; Nakatsuji, H.; Caricato, M.; Li, X.; Hratchian, H. P.; Izmaylov, A. F.; Bloino, J.; Zheng, G.; Sonnenberg, J. L.; Hada, M.; Ehara, M.; Toyota, K.; Fukuda, R.; Hasegawa, J.; Ishida, M.; Nakajima, T.; Honda, Y.; Kitao, O.; Nakai, H.; Vreven, T.; Montgomery, J. A., Jr.; Peralta, J. E.; Ogliaro, F.; Bearpark, M. J.; Heyd, J.; Brothers, E. N.; Kudin, K. N.; Staroverov, V. N.; Kobayashi, R.; Normand, J.; Raghavachari, K.; Rendell, A. P.; Burant, J. C.; Iyengar, S. S.; Tomasi, J.; Cossi, M.; Rega, N.; Millam, N. J.; Klene, M.; Knox, J. E.; Cross, J. B.; Bakken, V.; Adamo, C.; Jaramillo, J.; Gomperts, R.; Stratmann, R. E.; Yazyev, O.; Austin, A. J.; Cammi, R.; Pomelli, C.; Ochterski, J. W.; Martin, R. L.; Morokuma, K.; Zakrzewski, V. G.; Voth, G. A.; Salvador, P.; Dannenberg, J. J.; Dapprich, S.; Daniels, A. D.; Farkas, Ö.; Foresman, J. B.; Ortiz, J. V.; Cioslowski, J.; Fox, D. J. *Gaussian 09*; Gaussian, Inc.: Wallingford, CT, 2009.
(32) Chai, J.-D.; Head-Gordon, M. *Phys. Chem. Chem. Phys.* **2008**, *10*, 6615.
(33) Tomasi, J.; Mennucci, B.; Cammi, R. *Chem. Rev.* **2005**, *105*, 2999.
(34) Marenich, A. V.; Cramer, C. J.; Truhlar, D. G. *J. Phys. Chem. B* **2009**, *113*, 6378.
(35) In *Apex II Suite*; Bruker AXS Ltd.: Madison, WI, 2006.
(36) In *APEXII v2008*, 4-0 ed.; Bruker-Nonius Inc.: Madison, WI, 2008.
(37) Barbour, L. J. *J. Supramol. Chem.* **2003**, *1*, 189.
(38) Tate, B. K.; Wyss, C. M.; Bacsa, J.; Kluge, K.; Gelbaum, L.; Sadighi, J. P. *Chem. Sci.* **2013**, *4*, 3068.
(39) Haack, P.; Limberg, C.; Tietz, T.; Metzinger, R. *Chem. Commun.* **2011**, *47*, 6374.
(40) Shannon, R. *Acta Crystallogr., Sect. A* **1976**, *32*, 751.
(41) Bondi, A. *J. Phys. Chem.* **1964**, *68*, 441.
(42) Willcocks, A. M.; Robinson, T. P.; Roche, C.; Pugh, T.; Richards, S. P.; Kingsley, A. J.; Lowe, J. P.; Johnson, A. L. *Inorg. Chem.* **2011**, *51*, 246.
(43) Coucouvanis, D.; Kanodia, S.; Swenson, D.; Chen, S. J.; Stuedemann, T.; Baenziger, N. C.; Pedelty, R.; Chu, M. *J. Am. Chem. Soc.* **1993**, *115*, 11271.
(44) Cardell, D.; Hogarth, G.; Faulkner, S. *Inorg. Chim. Acta* **2006**, *359*, 1321.
(45) Camus, A.; Marsich, N.; Manotti Lanfredi, A. M.; Ugozzoli, F. *Inorg. Chim. Acta* **1989**, *161*, 87.
(46) Wycliff, C.; Bharathi, D. S.; Samuelson, A. G.; Nethaji, M. *Polyhedron* **1999**, *18*, 949.
(47) Lane, A. C.; Barnes, C. L.; Vollmer, M. V.; Walensky, J. R. *Inorganics* **2014**, *2*, 540.
(48) Victoriano, L. I.; Garland, M. T.; Vega, A.; Lopez, C. *Inorg. Chem.* **1998**, *37*, 2060.
(49) Kawajiri, R.; Okubo, T.; Mitani, T. *Polyhedron* **2006**, *25*, 2650.
(50) Liao, P.-K.; Fang, C.-S.; Edwards, A. J.; Kahlal, S.; Saillard, J.-Y.; Liu, C. W. *Inorg. Chem.* **2012**, *51*, 6577.
(51) Zhang, Q.; Cao, R.; Hong, M.; Su, W.; Liu, H. *Inorg. Chim. Acta* **1998**, *277*, 171.
(52) Huang, Z.; Lei, X.; Hong, M.; Liu, H. *Inorg. Chem.* **1992**, *31*, 2990.
(53) Liu, C. W.; Liao, P.-K.; Fang, C.-S.; Saillard, J.-Y.; Kahlal, S.; Wang, J.-C. *Chem. Commun.* **2011**, *47*, 5831.
(54) Ebihara, M.; Tokoro, K.; Imaeda, K.; Sakurai, K.; Masuda, H.; Kawamura, T. *Chem. Commun.* **1992**, 1591.
(55) Heese, R.; Nilson, L *Acta Chem. Scand.* **1969**, *23*, 825.
(56) Pandey, S.; Kane, M. A.; Baker, G. A.; Bright, F. V.; Fuerstner, A.; Seidel, G.; Leitner, W. *J. Phys. Chem. B* **2002**, *106*, 1820.
(57) Baker, G. A.; Wenner, B. R.; Watkins, A. N.; Bright, F. V. *J. Sol-Gel Sci. Technol.* **2000**, *17*, 71.
(58) Bukowski, R. M.; Ciriminna, R.; Pagliaro, M.; Bright, F. V. *Anal. Chem.* **2005**, *77*, 2670.